

Preparation and Characterization of a Bilayer Cr-C/Ni-P Coating on Aluminum 5052 as Bipolar Plates

Hsiang-Cheng Wang¹, Hung-Hua Sheu², Kung-Hsu Hou^{3,*}, Shun-Yi Jian², Ming-Hsien Lin², Ming-Der Ger^{2,*}

¹ Planning Division, National Chung-Shan Institute of Science & Technology, Taoyuan 325, Taiwan

² Department of Chemical & Materials Engineering, Chung Cheng Institute of Technology, National Defense University, Taoyuan 335, Taiwan

³ Department of Power Vehicle and Systems Engineering, Chung Cheng Institute of Technology, National Defense University, Taoyuan 335, Taiwan

*E-mail: mingderger@gmail.com, khou@ndu.edu.tw

Received: 1 March 2017 / Accepted: 17 April 2017 / Published: 12 May 2017

Aluminum alloy materials, with their light-weight and low-cost characteristics, are considered to be some of the most suitable materials for use as bipolar plates (BPPs). In this study, a chromium-carbon/nickel-phosphorus (Cr-C/Ni-P) bilayer coating is deposited on aluminum alloy 5052 (AA5052) to improve the corrosion resistance and interfacial contact resistance. An electroless Ni-P layer is initially deposited on the AA5052 to form an undercoat, onto which a Cr-C coating is subsequently deposited by electroplating from a trivalent chromium bath. The surface morphology and chemical composition of the prepared coatings were investigated using scanning electron microscopy (SEM) and electron probe X-ray micro-analyzer (EPMA) techniques. The surface morphology of the Cr-C coating that formed with a plating time of 10 min is smooth and crack- and pinhole-free; however, cracks and pinholes are clearly observed in deposits that have been plated for a longer plating time. Therefore, the potentiodynamic test results indicate that the coating prepared at 10 A dm⁻² and 10 min possesses the best corrosion resistance ($i_{\text{corr}} = 6.7 \times 10^{-7}$ A cm⁻²). The contact resistance of the Cr-C coating plated at 10 min is the lowest (8.2 mΩ·cm²). The aluminum BPPs that have a Cr-C/Ni-P bilayer coating exhibits great potential for PEMFC applications.

Keywords: Electroplating; Cr-C coating; Corrosion resistance; Aluminum bipolar plates; PEMFC

1. INTRODUCTION

Fuel cells, energy conversion devices with high efficiency, low noise, low pollutant emissions, high power density, without requiring charging for prolonged usage, are attracting more and more attention in recent years due to the growing concerns of climate change and the depletion of

petroleum-based energy resources [1-6]. Because of their potential as a clean, efficient, and reliable power source that can be operated at low temperatures, proton exchange membrane fuel cells (PEMFCs) are regarded as one of the most useful types of fuel cells for transportation, portable power and household power plant applications [7-10].

The bipolar plate (BPPs), which accounts for most of the total stack weight and cost of PEMFCs, is a significant multifunctional component of the PEMFC stack. The materials for BPPs can be divided into three categories: namely graphite, metallic and composite materials [11-14]. In the past, the graphite was commonly used because of its excellent conductivity and corrosion resistance. However, the intrinsic brittle nature, heavy weight, large volume, poor mechanical strength and expansive cost hinder the commercial applications of graphite BPPs [1,2]. On the contrary, metal plates have good ductility, electrical conductivity, machinability, and low cost. Therefore, metal plates have been studied as alternative BPPs materials for PEMFCs. In particular, aluminum is a promising metal for use in BPPs with its light-weight, low-density and low-cost characteristics [15]. Nevertheless, metallic materials are susceptible to corrosion under the acidic (pH 2-3) and humid operating conditions of PEMFCs. Corrosion can cause the formation of a passive film that increases the interfacial contact resistance (ICR) between a BPP and an electrode. In addition, the leaching of ions can poison the membrane electrode resulting in decreased cell performances [16-18]. Hence, a possible solution for using metal BPPs is to select an appropriate surface modification to enhance corrosion resistance while maintaining surface conductive. Many recent reports have revealed that chromium carbide exhibits a good corrosion resistance and an excellent surface conductivity.

Compared with other techniques for preparing Cr-C coatings [19,20], such as PBAIP, CVD and pack cementation, etc., the advantages of electroplating possesses including cheaper cost, easier operation, higher productivity, small and less geometric limitations. In our previous work [21,22], Cr-C coatings were successfully deposited on SS304 by electroplating from a trivalent Cr bath under different plating conditions. Our results showed that both the corrosion resistance and the ICR of the Cr-C coatings prepared by electrodeposition satisfy the goal set by the Department of Energy (DOE) for BPPs applications. However, aluminum is very reactive and has a great affinity for oxygen. When it is exposed to air, direct oxidation causes the spontaneous formation of a thin, compact, tough and inert oxide film on the surface of the aluminum leading to difficulty with electrodeposition onto its surface. Therefore, special pretreatment sequences are essential to enable aluminum substrates to be electroplated with adherent coatings. Zincating by immersion is the most widely used pretreatment technique used prior to the electrodeposition of metallic coatings on aluminum [23]. However, our unpublished results showed that the zincating pretreatment is not sufficient for producing a qualified electrodeposited Cr-C coating on a zincate-coated 5052 aluminum alloy. It can be ascribed to the very poor throwing power of the chromium coating. The reasons for that are not well-understood; nevertheless, it is evident that the use of a proper pretreatment method should be considered for the electrodeposition of a Cr-C coating on aluminum.

It has been reported that a Ni-P coating can be deposited on zincate-coated aluminum alloys [24-27]. Lin et al. [24] deposited a Ni-P coating on aluminum by electroless deposition and indicated that the Ni-P-coated aluminum BPP was more hydrophobic and had a corrosion current density 1 order of magnitude lower than that of the bare plate. Fetohi et al. [25] deposited Ni-P and Ni-Mo-P coatings

on aluminum alloy 6061 using electroless and electroplating deposition techniques. Both Ni-P- and Ni-Mo-P-coated AA6061 show a lower ICR value and a higher corrosion resistance when compared to bare aluminum alloy. Moreover, Voorwald et al. [26] reported that the presence of an electroless nickel interlayer increased the fatigue strength of hard chromium electroplated AISI 4340 steel.

Therefore, an electroless Ni-P undercoat was applied to pretreated aluminum alloys prior to the electrodeposition from a trivalent chromium bath to enhance the corrosion resistance and improve the coating adherence in this study. The electrodeposition of the Cr-C coatings was carried out at a constant current density (10 A dm^{-2}) and varying deposition times to investigate the effects of plating time on the contact and corrosion resistances of the Cr-C/Ni-P-coated aluminum alloy.

2. MATERIALS AND METHODS

2.1. Preparation of materials

Al-alloy 5052 with a surface roughness (R_a) of approximately $0.28 \mu\text{m}$ was used as the substrate material of BPPs in this experiment. Al alloy 5052 sheets of $50 \text{ mm (L)} \times 50 \text{ mm (W)} \times 2 \text{ mm (T)}$ were polished with silicon-carbide abrasive paper, pickled in acid solution for 30 seconds and activated with a 30 g L^{-1} NaOH aqueous solution. Prior to the electroless plating of a Ni-P undercoat, the zincating process was repeated twice using an immersion technique. The chemical composition of the zincate solution is presented in Table 1, whereas the immersion time was approximately 1 min and the temperature was $25 \text{ }^\circ\text{C}$. Between the two zincating processes, AA5052 was immersed in a nitric acid solution (30% HNO_3) for 2 min and cleaned with deionized water. Then, the AA 5052 substrates were immersed in the Ni-P electroless bath at 85°C for 10 minutes to deposit an electroless-plated Ni-P coating on the substrates. The surface morphology and roughness of the pre-treated specimen is shown in Fig. 1.

Table 1. The chemical composition of zincate bath.

Bath composition	Concentration
NaOH	12.5 M
ZnO	0.92 M
$\text{FeCl}_3 \cdot 6\text{H}_2\text{O}$	0.0037 M
NaNO_3	0.012 M
$\text{KNaC}_4\text{H}_4\text{O}_6 \cdot 4\text{H}_2\text{O}$	0.0071M

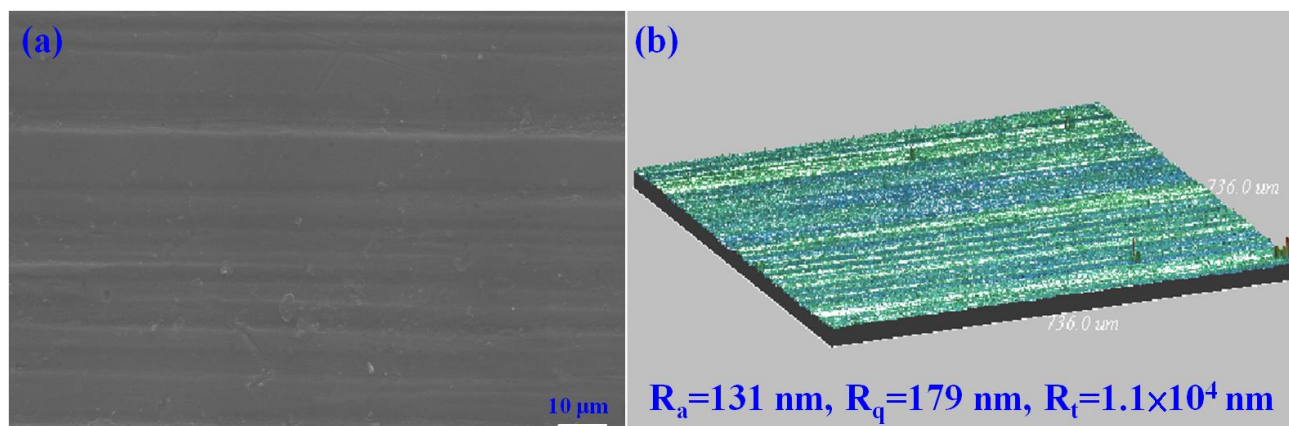


Figure 1. Surface morphology (a) and 3 D surface image (b) of Ni-P layer deposited on AA5052.

The electrodeposition process was used to deposit the Cr-C coatings on the pretreated specimens. The bath composition and conditions for preparing the Cr-C coatings in the present investigation were chosen based on our previous result [28]. The electroplating was performed at 10 A dm^{-2} for 10, 30 and 60 min, respectively. Various Cr-C/Ni-P bilayer coatings have been simply named as Cr-C(10)/Ni-P, Cr-C(30)/Ni-P and Cr-C(60)/Ni-P based on the plating times for the deposition of the Cr-C layer.

2.2. Sample Morphology and Elemental Composition

A field emission scanning electron microscope (FESEM, JEOL JEM-6700F) was employed to analyze the surface and cross-sectional morphologies of the Cr-C/Ni-P coatings on Al alloy 5052. The electron probe X-ray micro-analyzer (EPMA, JXA-8200) was used to investigate the distribution of Cr, C, and O in the coatings. A sub-nanometer 3D optical profiler (SNOP; Chroma 7502, Taiwan) was adopted to measure surface roughness of the specimen surfaces before and after corrosion test to examine the corrosion effects.

2.3. Interfacial contact resistance test

The ICR between the specimen and gas diffusion layer (GDL) was measured using a method similar to the one reported earlier [29,30]. For measuring the ICR, two pieces of carbon paper were sandwiched between the BPP sample and two copper plates. During the tests, a constant electrical current of 1 A was applied through the copper plates, and the voltage drop was recorded using a digital multimeter (M3500A, Picotest, USA). The variation in the total voltage was recorded with respect to the compaction force that was steadily increased from 0 to 200 N cm^{-2} and recorded every 10 N cm^{-2} increment. To investigate the effects of PEMFC corrosive conditions on the ICRs of the BPP samples, ICR tests were conducted before and after the corrosion tests.

2.4. Electrochemical analyses

Potentiodynamic and potentiostatic tests were conducted in a 0.5 M H₂SO₄ aqueous solution at 70°C using an Autolab PGSTAT30 potentiostat/galvanostat controlled by the GPES (General Purpose Electrochemical System) software. A typical three-electrode cell system was used. A platinum sheet and saturated calomel electrode (SCE, saturated KCl) was used as the counter electrode and the reference electrode, respectively. After the specimens were stabilized at the open circuit potential (OCP), the potential was swept with a scan rate of 5 mV s⁻¹. A potential of +0.6 V_{SCE} with air purged was used for potentiostatic test. The total time for one potentiostatic test was 10 hr. Furthermore, for the purpose of studying the difference in the quantity of metallic ions separated out from the electrolyte after potentiostatic testing, inductively coupled plasma-mass spectrometry (ICP-MS, Liberty Series II, USA) was adopted.

3. RESULTS AND DISCUSSION

3.1. Surface morphology, thickness and composition analysis of the Cr-C coatings

Fig. 2 shows the cross-sectional SEM images and thicknesses of the Cr-C layers electroplated at 10 A dm⁻² for different plating times. The thicknesses of the Cr-C layers estimated from Fig. 2 are approximately 2.1 μm, 3.8 μm and 4.9 μm after plating for 10, 30 and 60 minutes, respectively. As shown from these results, the thicknesses of the Cr-C layers increase with deposition time; furthermore, the deposition rate decreases significantly with time. It is known that the trivalent Cr ion exists in the form of a Cr(H₂O)₆³⁺ complex, which is very inactive in a simple trivalent Cr solution. The deposition of metal chromium using solutions based on Cr(III) can only be carried out with electrolytes containing organic acids, such as formic acid, ammonium formate, acetic acid and oxalic acid [31-37]. The carbon existing in these organic acids in the bath is incorporated in the coating and accompanies the reduced chromium metal. Therefore, the concentration of the formic acid plays an important role in the electroreduction of trivalent Cr [28]. The decrease in the deposition rate observed at the longer deposition times in the present study was likely a result of the continuous decrease in the concentration of the complexing agent in the bath as the electrodeposition continued. Moreover, the increase in the pH near the cathode resulting from the hydrogen evolution causes an oxidation reaction and the formation of a Cr oxidation product, which further prevents the reduction of the Cr ions [38,39].

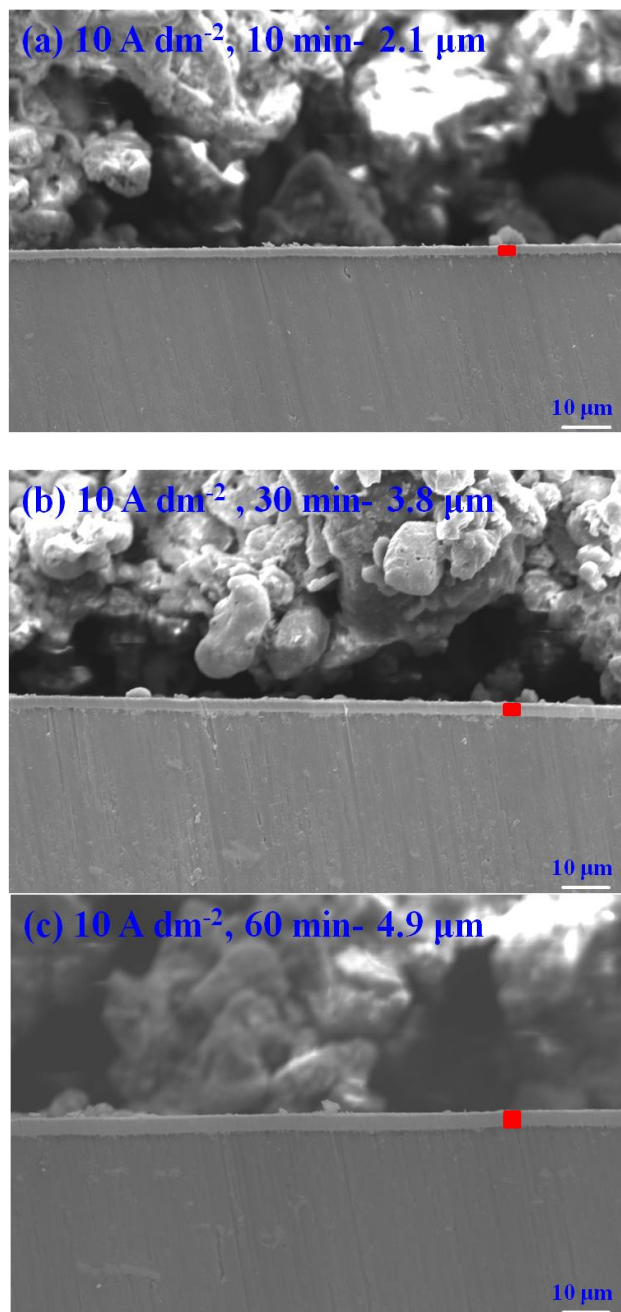


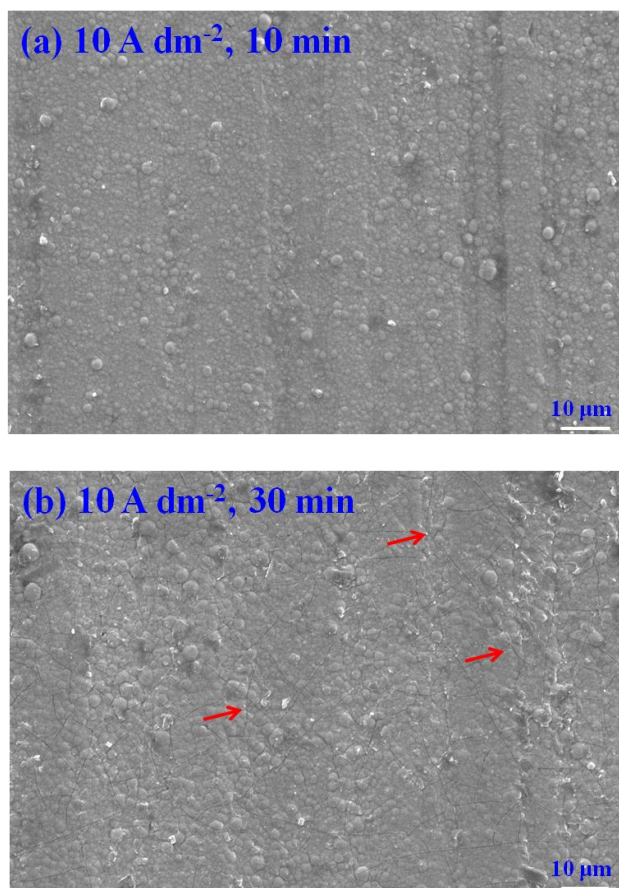
Figure 2. The cross-sectional SEM images of the Cr-C coated AA5052 from electroplating for different times: (a) 10 A dm⁻², 10 min; (b) 10 A dm⁻², 30 min; and (c) 10 A dm⁻², 60 min.

The compositions of the coatings are listed in Table 2. The C content and O content decreased with increasing plating time. Approximately 41.8 at% of C and 0.6 at% of O was deposited when the plating time was 10 min. When plating for 30 and 60 min, the C and O content in the coating decreased significantly to 30.1 at% and 0.5 at%, and 24.8 at% and 0.3 at%, respectively. This result is likely attributed to a decrease in the concentration of formic acid during the electrodeposition.

Table 2. The composition of the Cr-C layer electroplated for different time at 10 A dm⁻².

Plating time	EPMA (at.%)		
	Cr	C	O
10 min	57.6	41.8	0.6
30 min	69.4	30.1	0.5
60 min	74.9	24.8	0.3

Fig. 3 shows the surface morphologies of the Cr-C/Ni-P-coated Al alloy 5052 electroplated at 10 A dm⁻² for different plating times. From the SEM images shown in Fig. 3(a), no obvious pinhole is observed, and the Cr-C film prepared by plating for 10 min is dense, continuous and compact, indicating that the Cr-C coating can block the substrate from direct corrosion. When plating for 30 min and 60 min, it clearly shows that micro-crack networks appeared in the chromium deposited onto Al 5052, and the micro-cracks became wider and deeper with an increase in the plating time. The presence of micro-cracks at a longer plating time likely results from residual tensile stress, which increases with the thickness of coating. The results obtained in the present study showing that micro-cracks increased with increasing plating time is consistent with the literature report for the electroplating of Cr-P coatings [40].



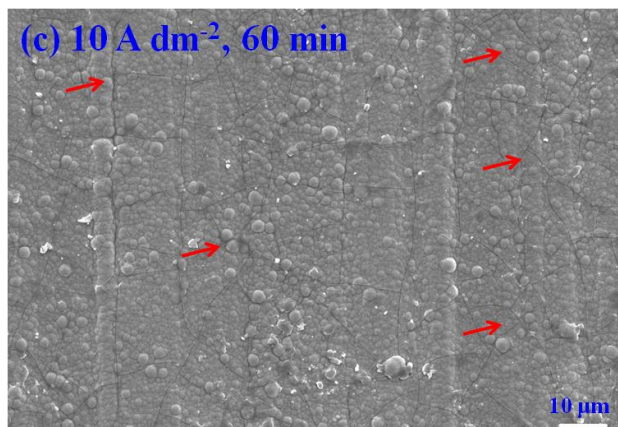


Figure 3. The surface morphology of the Cr-C coated AA5052 obtaining from electroplating for different plating times: (a) 10 min; (b) 30 min; and (c) 60 min.

Fig. 4 shows 3D surface images of Cr-C coatings on Al alloy 5052. The data of surface roughness are listed in Table 3. The 3D images illustrated that the surface topographies vary with plating times. The root mean square roughness (R_q) of the Ni-P undercoat is 179 nm. The R_q of the Cr-C/Ni-P coatings for plating time of 10, 30 and 60 min was 198 nm, 212 nm and 221 nm, respectively (Table 3). It is evident that the surface roughness of Cr-C coatings increased with the plating time, which is consistent with the results in Fig. 3. Compared to our previous results on the electrodeposition of Cr-C coatings on ss304 [22], the roughness in the present investigation for the Cr-C/Ni-P-coated Al alloy 5052 is higher than that of the Cr-C-coated ss304 plated using the same conditions. This result suggests that the surface roughness of the Cr-C coating may be influenced by the Ni-P undercoat because the roughness was much lower in the ss304 (50 nm) than for the Ni-P undercoat (179 nm)..

Table 3. The surface roughness of the Cr-C/Ni-P coated AA 5052 formed by electroplating at 10 A dm^{-2} for different plating times.

Plating time	Surface Roughness (nm)		
	Ra	Rq	Rt
10 min	146	198	1.2×10^4
30 min	157	212	7.6×10^3
60 min	164	221	1.3×10^4

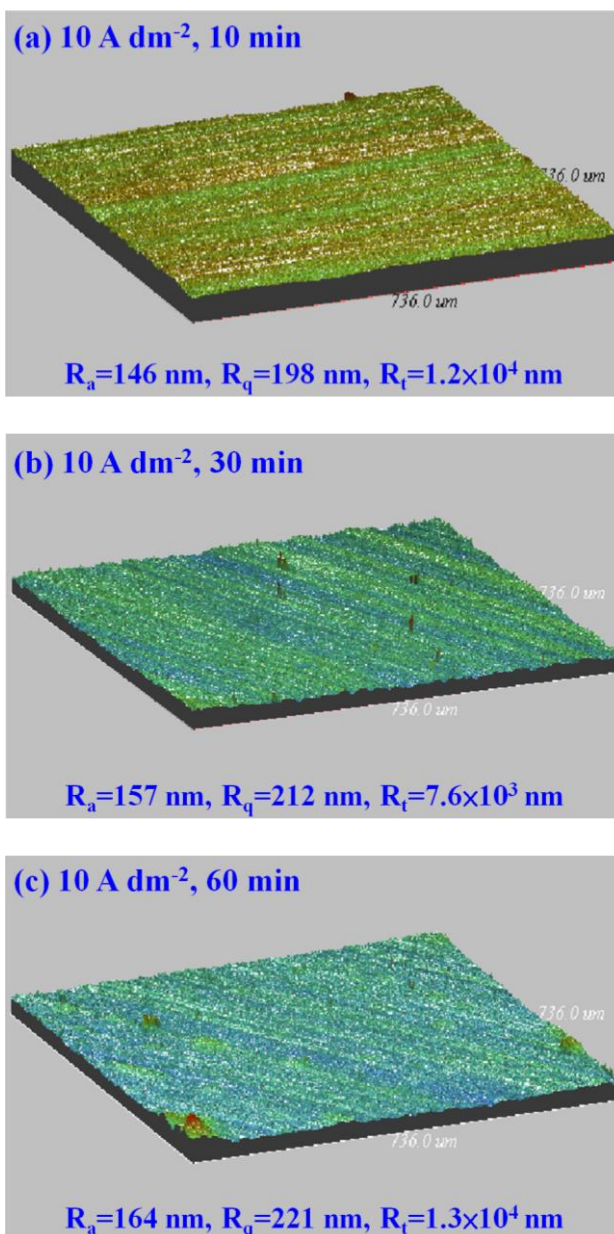


Figure 4. 3D surface images of specimens obtained from optical profilometer for Cr-C coatings on AA5052 produced from electroplating for different times.

It's observed that the surface roughness of the Cr-C coating increased with the plating time, which is consistent with the results in Fig. 3. Compared to our previous results on the electrodeposition of Cr-C coatings on ss304 [24], the roughness in the present investigation for the Cr-C/Ni-P-coated Al alloy 5052 is higher than that of the Cr-C-coated ss304 plated using the same conditions. The results also show that the surface roughness of the Cr-C coating may be influenced by the Ni-P undercoat because the roughness was much lower in the ss304 (50 nm) than for the Ni-P undercoat (179 nm).

3.2 Potentiodynamic and potentiostatic polarization

Fig. 5 shows the potentiodynamic polarization results of the Ni-P-coated and Cr-C/Ni-P-coated Al alloy 5052 samples in a 0.5 M H₂SO₄ solution at 70°C. The corrosion potentials (E_{corr}) and corrosion current densities (i_{corr}) were evaluated and listed in Table 4. The E_{corr} and i_{corr} of the Ni-P-coated specimen is approximately -556 mV vs. SCE and 3.1×10^{-6} A cm⁻², respectively. The i_{corr} of the Ni-P-coated Al alloy in present study is comparable to those reported in literatures for the modified Al alloys with electroplated as well as electroless plated Ni-P coatings [2,7-8,11,24-25,27]. The E_{corr} values of the Cr-C/Ni-P-coated specimens prepared at various plating times are higher and the i_{corr} values of the Cr-C/Ni-P-coated specimens are much lower than those of the Ni-P-coated specimen. These results reveal that the corrosion resistance of the Cr-C coatings is better than that of the Ni-P-coated specimen. Moreover, it should be mentioned that the i_{corr} of the Cr-C(10)/Ni-P coating is the lowest whereas its E_{corr} is the highest among all tested specimens. Apparently, the corrosion resistance of Cr-C(10)/Ni-P is superior to those deposited for a longer time (Cr-C(30)/Ni-P and Cr-C(60)/Ni-P). The superior corrosion protection provided by Cr-C(10)/Ni-P, which can be attributed the coating having fewer micro-cracks as well as a relatively uniform structure, decreases the pathways for the destructive Cl⁻ anions to enter into the coating. The i_{corr} value of Cr-C(10)/Ni-P is the lowest value, 6.7×10^{-7} A cm⁻², which is well below the recommended upper limit value of 1.0×10^{-6} A cm⁻² given by the U.S. DOE 2020 technical targets for BPPs of PEMFCs [41].

Table 4. Comparison of the electrochemical parameters (E_{corr} and i_{corr}) of potentiodynamic polarization curves recorded in 0.5 M H₂SO₄ solution at 25 °C for the Ni-P and the Cr-C/Ni-P coated AA5052 electrodeposited for different times at 10 A dm⁻².

i_{corr} & E_{corr}	Al 5052+ Ni-P	Plating time		
		10 min	30 min	60 min
i_{corr} (A cm ⁻²)	3.1×10^{-6}	6.7×10^{-7}	7.8×10^{-7}	2.1×10^{-6}
E_{corr} (mV)	-556	-81	-112	-165

To understand the effects of coating aluminum with Cr-C on their stability against corrosion in the operation conditions of PEMFCs, the potentiostatic polarization technique was applied using a 0.5 M H₂SO₄ solution at 70°C for 10 h. The potential of 0.6 V_{SCE} was loaded and air was purged to simulate the cathodic environment of PEMFCs. Fig. 6 shows the variation in the current density as a function of time for the Ni-P- and Cr-C(10)/Ni-P-coated substrates. For all tested specimens, the current density decreased at the beginning of the polarization.

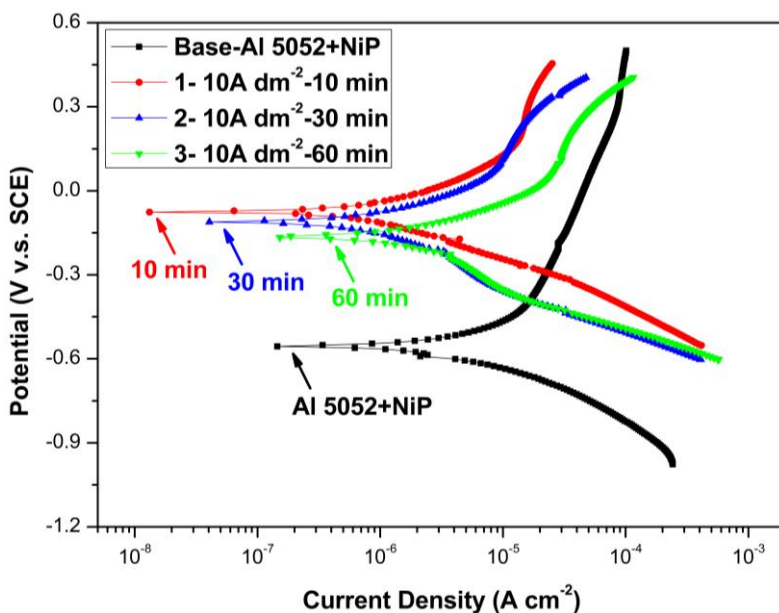


Figure 5. Potentiodynamic polarization curve of the Ni-P and Cr-C/Ni-P coated AA 5052 specimens in 0.5 M H₂SO₄ solution with a scan rate of 5 mV s⁻¹.

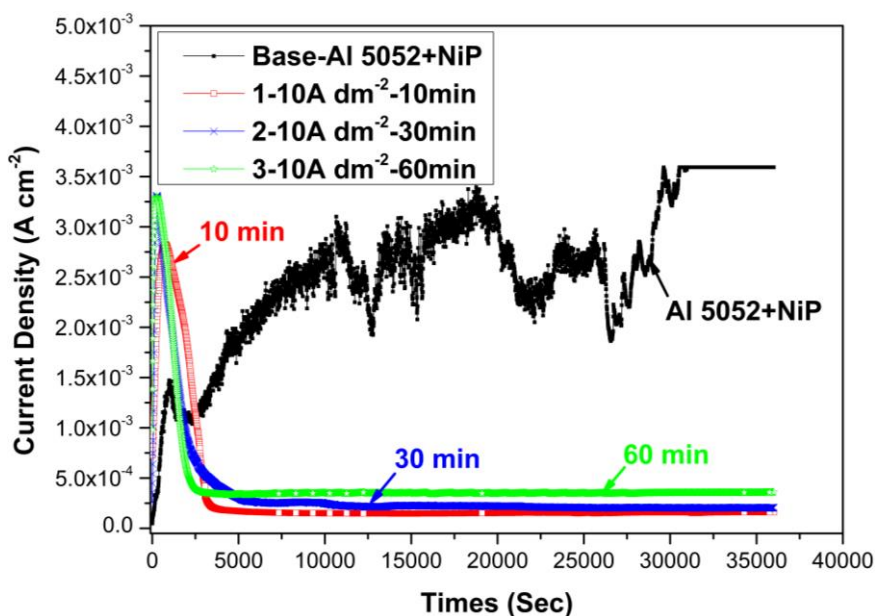


Figure 6. Potentiostatic polarization curves of Ni-P and Cr-C/Ni-P coated AA5052 samples at 0.6 V versus SCE in 0.5 M H₂SO₄ solution with air purging for 10 h.

Afterwards, the current density gradually stabilized in the Cr-C(10)/Ni-P-coated AA5052 specimens over the whole studied period. This may be related to the coverage of the entire coated surface by a passive film. However, the Ni-P-coated sample showed an abrupt increase in the current density after 1,197 s from the start of polarization until 30,674 s, and then it stabilized. The pinholes and defects in the Ni-P coating provides channels for corrosive mediums to directly make contact with the AA-5052 substrate leading to serious corrosion. The current density of the Cr-C(10)/Ni-P-coated

samples was approximately two orders of magnitude lower than that of the Ni-P-coated sample. According to the above results, the Cr-C coating on Ni-P pretreated AA5052 effectively protected it against corrosion for long time. In particular, Cr-C(10)/Ni-P exhibited the lowest current density during the entire test, indicating that the coating is most stable in the cathodic environment. This observation coincides well with the results obtained using the potentiodynamic polarization technique.

The solutions following the 10 h potentiostatic test were carefully collected, and the concentration of metal ions dissolved due to corrosion was analyzed by ICP. The contents of Cr, Ni and Al, which are the major metallic elements of Cr-C coating, Ni-P undercoat and AA5052, were recorded for Ni-P-coated and Cr-C(10)/Ni-P-coated AA5052 samples in the simulated cathode environment, and the results are presented in Table 5. The total metal ion concentrations leached from the Ni-P pretreated specimen are approximately 66.4 ppm after 10 h potentiostatic test in the simulated PEMFC cathode environments and only 13.9 ppm for the Cr-C coated specimen electroplated for plating time of 10 min. Compared to Cr-C(10)/Ni-P, the metal ion concentrations of the Cr-C(30)/Ni-P and Cr-C(60)/Ni-P coatings are higher, and this trend is consistent with the potentiodynamic results. Overall, the potentiodynamic and ICP results indicate that the Cr-C(10)/Ni-P coating indeed shows outstanding performance for anticorrosion applications.

Table 5. Metal ions concentration leached from the Ni-P and Cr-C/Ni-P coated AA5052 samples after 10 h potentiostatic test.

Ions	Ni-P coated AA5052	Cr-C(10)/Ni-P coated AA5052	Cr-C(30)/Ni-P coated AA5052	Cr-C(60)/Ni-P coated AA5052
Cr	1.8	0.1	0.1	0.1
Ni	59.8	11.9	23.5	35.3
Al	4.8	1.9	2.2	3.6
Total	66.4	13.9	25.8	39.0

Unit: ppm

3.3 Surface morphology after potentiostatic test

The surface morphology of the Ni-P-coated specimen and the Cr-C/Ni-P-coated Al alloy 5052 specimens electroplated by different plating times following the 10 h potentiostatic test at 0.6 V_{SCE} with air purging in 0.5 M H₂SO₄ solution is displayed in Fig. 7. Fig. 7(a) shows that a large piece of coating peeled off the surface of the Ni-P-coated AA5052. This result indicates that the Ni-P-coated AA-5052 had a poor corrosion resistance in the PEMFC cathode environment. However, for Cr-C(10)/Ni-P-coated AA-5052 specimens, some cavities appear on the surface, indicating the presence of pitting corrosion on the surface of the Cr-C coatings in the simulated cathodic environment. However, the extent of the corrosion of the Ni-P coating is more severe than that of the Cr-C-coated samples.

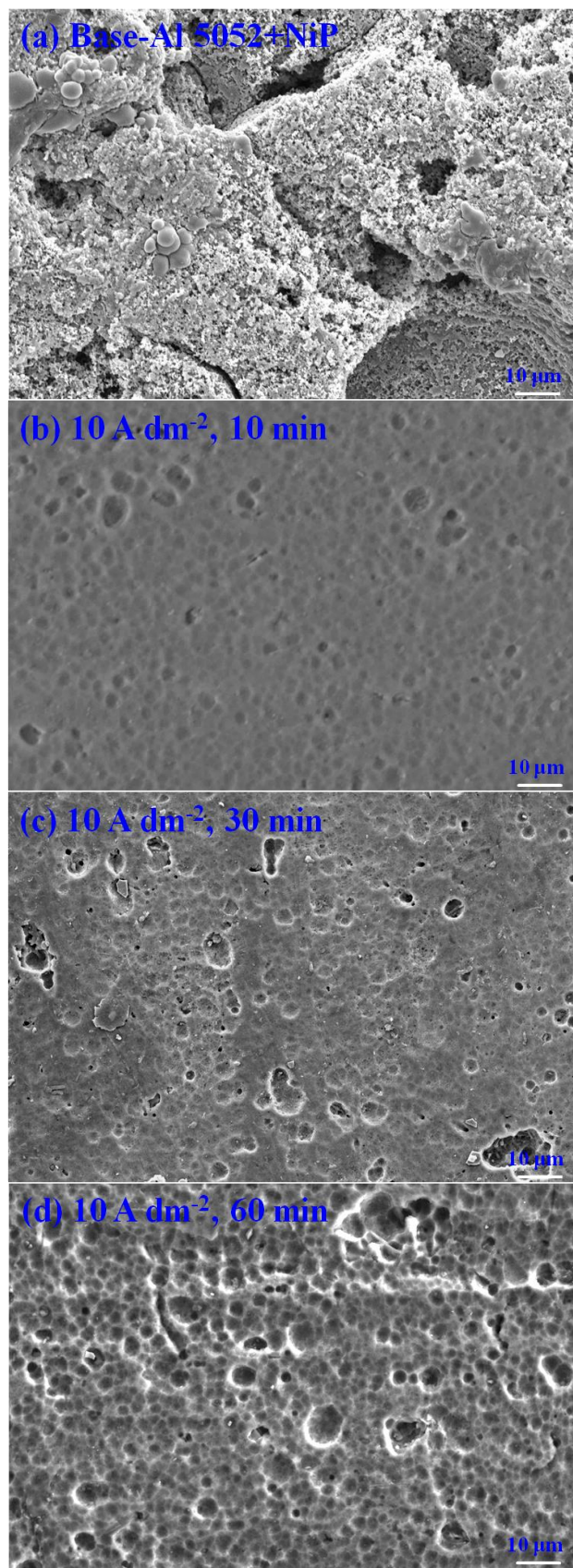


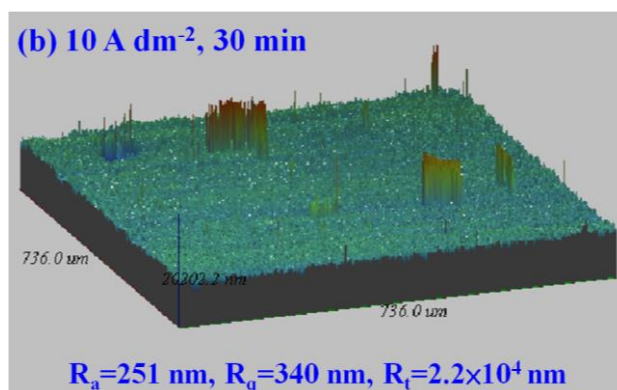
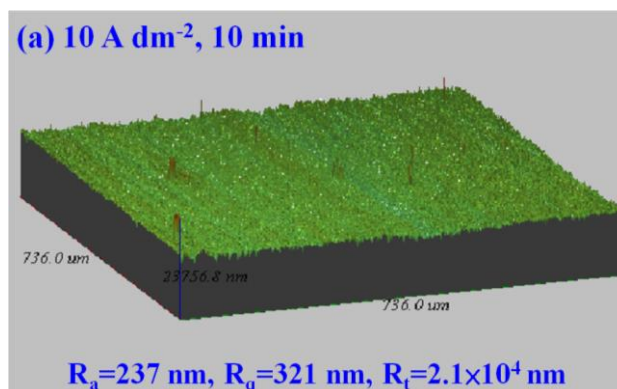
Figure 7. The surface morphology of the Ni-P and Cr-C/Ni-P coated AA5052 electroplated with different plating times after potentiostatic test.

On the other hand, careful inspection of Fig. 7(b), 7(c) and 7(d) shows that an increase in the number and size of the micro-voids, which can be used as an indication of the extent of corrosion, is evident for Cr-C(30)/Ni-P and Cr-C(60)/Ni-P as a result of localized corrosion attacks. The surface morphology of the Cr-C(10)/Ni-P, among all of the three, revealed the least corrosion, which is consistent with the results of corrosion testing.

The surface roughness of the Cr-C/Ni-P-coated Al alloy 5052 electrodeposited for different plating times at 10 A dm⁻² after potentiostatic test is displayed in Fig. 8. The surface roughness of Cr-C coatings after potentiodynamic testing is listed in Table 6. Comparing Table 3 and 6, it can be clearly seen that the mean surface roughness of Cr-C coatings after potentiodynamic testing is larger than that before potentiodynamic testing. It might be ascribed to the formation of cavities caused by corrosion.

Table 6. The surface roughness of the Cr-C/Ni-P coated AA5052 electrodeposited for different plating times at 10 A dm⁻² after potentiostatic test.

Plating time	Surface Roughness (nm) after Potentiostatic test		
	Ra	Rq	Rt
10 min	237	321	2.1×10 ⁴
30 min	251	340	2.2×10 ⁴
60 min	262	349	1.3×10 ⁴



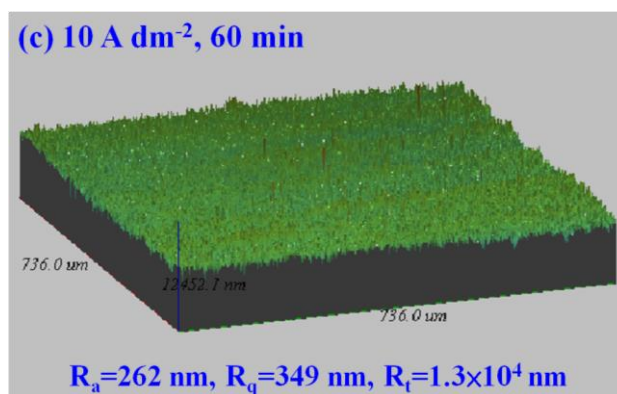


Figure 8. 3D surface images of Cr-C/Ni-P coated AA5052 specimens after potentiostatic test.

3.4 Interfacial contact resistance after potentiostatic test

A passive film made of a metallic oxide will form on the surface of the BPPs when they are exposed to the acidic and high temperature operation conditions of PEMFCs, leading to an increasing in the ICR. Therefore, a low ICR is also one of the most important requirements for BPPs.

The ICR values of all of the coated specimens show a similar trend: the ICR decreases rapidly with low compaction forces and then decreased gradually with high compaction forces. The measured ICR values were compared with the 2020 target ICR value (lower than 10 mΩ·cm² at 138 N cm⁻² compaction pressure) set by United States DOE for PEMFC applications [41]. These comparisons are shown in Fig. 9 at a standard compaction force value of 138 Ncm⁻² for different coatings before and after potentiostatic tests in a simulated cathode environment. ICR values of 63.3 and 139.2 mΩ·cm² were obtained, respectively, for the Ni-P-coated specimen at a compaction force of 138 N cm⁻² before and after potentiostatic testing. This can be attributed to the change of the nature of surface layer. When a passive film forms on the metal surface, it leads to an increase of the ICR. After coating the Ni-P-coated aluminum substrates with Cr-C, the ICR values decreased tremendously compared to the ICR value of the Ni-P-coated substrate. Cr-C(10)/Ni-P showed the lowest ICR value (8.2 mΩ·cm²) at a load of 138 N cm⁻² and fulfilled the desired value of DOE for the BPP applications. The ICR measurement results indicated that the Cr-C(10)/Ni-P coating had excellent electrical conductivity compared to Cr-C(30)/Ni-P and Cr-C(60)/Ni-P coatings.

As shown in Fig. 9, the ICR values of all of the test specimens increased at the same compaction force after potentiodynamic polarization for 10 h in a simulated PEMFC environment. However, the increase in the ICR for the Cr-C/Ni-P-coated AA5052 is much smaller than that for the Ni-P-coated specimen after a similar corrosion test, illustrating the beneficial effect of the Cr-C layer against the corrosion of AA5052.

The ICR value of the Cr-C(10)/Ni-P-coated AA5052 is 8.2 mΩ·cm² under 138 N cm⁻² which is slightly lower than that of our previous work (Cr-C coated SS304) [22]. The ICR is mainly influenced by the contact area between the sample and the carbon paper as well as the conductivity of the sample surface. The relatively smooth surface of Cr-C(10)/Ni-P increases the actual contact area between the fuel cell components, which in turn decrease the ICR [42]. However, based on the surface composition

of the Cr-C coatings, the Cr-C(10)/Ni-P coating contains 41.8 at.% C and the carbon content in Cr-C-coated SS304 electroplated for 10 min is 39 at.%. The Cr-C(10)/Ni-P coating has lower ICR as anticipated, which can be attributed to the good electrical conductivity of the outmost Cr-C layer.

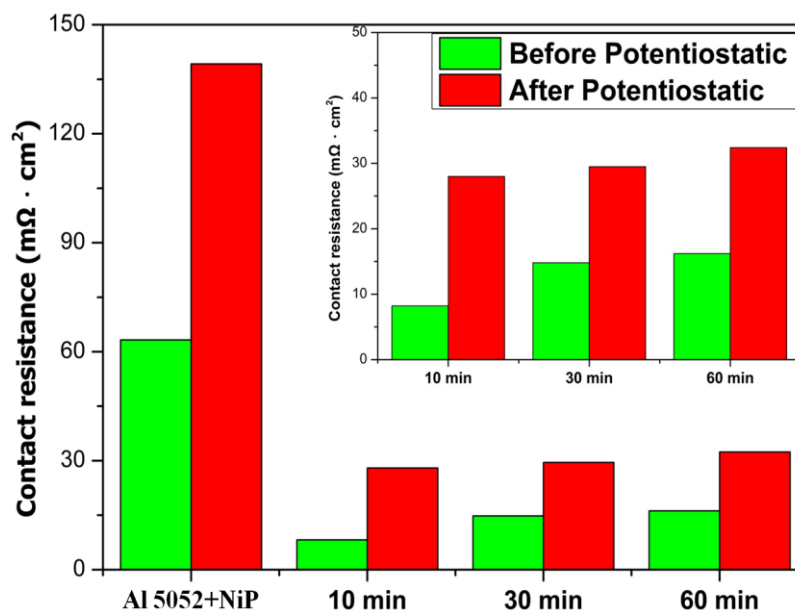


Figure 9. The ICR values (under 138 N cm^{-2}) of Ni-P and Cr-C/Ni-P coated samples before and after potentiostatic test in simulating cathode environment.

4. CONCLUSIONS

Using electroless Ni-P plated as an underlayer, Cr-C/Ni-P bilayer coatings can be successfully deposited on AA5052 substrates as BPPs for PEMFC applications. A smooth and pinhole-free layer forms when the plating time is short (10 min). The Cr-C coating was electrodeposited from a trivalent Cr bath for 10 min and showed the lowest ICR value of $8.2 \text{ m}\Omega \cdot \text{cm}^2$ at 138 N cm^{-2} , the lowest corrosion current density of $6.7 \times 10^{-7} \text{ A cm}^{-2}$. From the results, it can be concluded that the corrosion resistance and ICR values of the AA5052 substrate are greatly improved and reach the US DOE requirements with the aid of a surface Cr-C film. Moreover, the results indicate that the Cr-C-coated BPP is considerably stable and has better anti-corrosion ability than previous studies. Based on the results above, AA5052 substrates coated with a Cr-C(10)/Ni-P film have great potential as BPPs in PEMFC applications.

References

1. J. Wind, R. Späh, W. Kaiser and G. Böhm, *J. Power Sources*, 105 (2002) 256.
2. A. E. Fetohi, R. M. A. Hameed and K. M. El-Khatib, *J. Ind. and Eng. Chem.*, 30 (2015) 239.
3. H.C. Chien, L.D. Tsai, C.M. Lai, J.N. Lin, C.Y. Zhu, F.C. Chang, Characteristics of high-water-uptake activated carbon/Nafion hybrid membranes for proton exchange membrane fuel cells, *J. Power Sources* 226 (2013) 87–93.

4. H. Husby, O.E. Kongstein, A. Oedegaard, F. Seland, Carbonpolymer composite coatings for PEM fuel cell bipolar plates, *Int. J. Hydrogen Energy* 39 (2014) 951–957.
5. Y.C. Park, S.H. Lee, S.K. Kim, S. Lim, D.H. Jung, S.Y. Choi, J.H. Kim, D.H. Peck, Effects of CrN/Cr coating layer on durability of metal bipolar plates under a fuel recirculation system of direct methanol fuel cells, *Int. J. Hydrogen Energy* 38 (2013) 10567–10576.
6. K Sopian, WRW Daud, Challenges and future developments in proton exchange membrane fuel cells, *Renew. Energy* 31 (2006) 719–727.
7. J. R. Mawdsley, J. D. Carter, X. Wang, S. Niyogi, .C. Q. Fan, R. Koc and G. Osterhout, *J. Power Sources*, 231 (2013) 106.
8. S. Y. Tsai, C. Y. Bai, C. H. Lin, G. N. Shi, K. H. Hou, Y. M. Liu and M. D. Ger, *J. Power Sources*, 214 (2012) 51.
9. J.W. Lim, D.G. Lee, Carbon composite hybrid bipolar plates with bypass-connected gas diffusion layers for PEM fuel cells, *Compos. Struct.* 95 (2013) 557–563.
10. S. Karimi, N. Fraser, B. Roberts, F.R. Foulkes, A review of metallic bipolar plates for proton exchange membrane fuel cells: materials and fabrication methods, *Adv. Mater. Sci. Eng.* 2012 (2012) 1–22.
11. M. M. Sisan, M. A. Sereshki, H. Khorsand and M. H. Siadati, *J. Alloy Compd.*, 613 (2014) 288.
12. X. Li, I. Sabir, Review of bipolar plates in PEM fuel cells: Flow-field designs, *Int. J. Hydrogen Energy* 30 (2005) 359–371.
13. R.F. Silva, A. Pozio, Corrosion Study on Different Types of Metallic Bipolar Plates for Polymer Electrolyte Membrane Fuel Cells, *J. Fuel Cell Sci. Technol.* 4 (2006) 116–122.
14. R.F. Silva, D. Franchi, A. Leone, L. Pilloni, A. Masci, A. Pozio, Surface conductivity and stability of metallic bipolar plate materials for polymer electrolyte fuel cells, *Electrochim. Acta* 51 (2006) 3592–3598.
15. B. D. Mert, *Corros. Sci.*, 103 (2016) 88.
16. M. Kumagai, S. T. Myung, S. Kuwata, R. Asaishi and H. Yashiro, *Electrochim. Acta*, 53 (2008) 4205.
17. H. Tawfik, Y. Hung and D. Mahajan, *J. Power Sources*, 163 (2007) 755.
18. Z. Li, K. Feng, Z. Wang, X. Cai, C Yao and Y. Wu, *Int. J. Hydrogen Energy*, 39 (2014) 8421.
19. Y. Zhao, L. Wei, P. Yi and L. Peng, *Int. J. Hydrogen Energy*, 41 (2016) 1142.
20. B. Wu, G. Lin, Y. Fu, M. Hou and B. Yi, *Int. J. Hydrogen Energy*, 35 (2010) 13255.
21. H. C. Wang, K. H. Hou, C. E. Lu and M. D. Ger, *Thin Solid Films*, 570 (2014) 209.
22. H. C. Wang, H. H. Sheu, C. E. Lu, K. H. Hou and M. D. Ger, *J. Power Sources*, 293 (2015) 475.
23. M. Hino, K. Murakami, Y. Mitooka, K. Muraoka, R. Furukawa and T. Kanadani, *Mater. Trans.*, 50 (2009) 2235.
24. C. H. Lin and S. Y. Tsai, *Appl. Energy*, 100 (2012) 87.
25. A. E. Fetohi, R. M. A. Hameed and K. M. El-Khatib, *J. Power Sources*, 240 (2013) 589.
26. H. J. C. Voorwald, R. Padilha, M. Y. P. Costa, W. L. Pigatin and M. O. H. Cioffi, *Int. J. Fatigue*, 29 (2007) 695.
27. A. E. Fetohi, R. M. A. Hameed, K. M. El-Khatib and E. R. Souayac, *Int. J. Hydrogen Energy*, 37 (2012) 7677.
28. C. E. Lu, N. W. Pu, K. H. Hou, C. C. Tseng and M. D. Ger, *Appl. Surf. Sci.*, 282 (2013) 544.
29. D. P. Davies, P. L. Adcock, M. Turpin and S. J. Rowen, *J. Power Sources*, 86 (2000) 237.
30. H. Wang, M. A. Sweikart and J. A. Turner, *J. Power Sources*, 115 (2003) 243.
31. Z. Zeng, Y. Sun and J. Zhang, *Electrochem. Commun.*, 11 (2009) 331.
32. S. C. Kwon, M. Kim, S. U. Park, D. Y. Kim, D. Kim, K. S. Nam and Y. Choi, *Surf. Coat. Technol.*, 183 (2004) 51.
33. G. Saravanan and S. Mohan, *Corros. Sci.*, 51 (2009) 197.
34. S. Ghaziof, M. A. Golozar and K. Raeissi, *J. Alloy. Compd.*, 496 (2010) 164.
35. S. Hoshino, H. A. Laitinen and G. B. Hoflund, *J. Electrochem. Soc.*, 133 (1986) 681.

36. S. Survilienė, O. Nivinskienė, A. Češunienė and A. Selskis, *J. Appl. Electrochem.*, 36 (2006) 649.
37. G. B. Hoflund, A. L. Grogan, D. A. Asbury, H. A. Laitinen and S. Hoshino, *Appl. Surf. Sci.*, 28 (1987) 224.
38. V. Zin and M. Dabalà, *Acta Mater.*, 58 (2010) 311.
39. J. Degenhardt and A. J. McQuillan, *Chem. Phys. Lett.*, 311 (1999) 179.
40. B. Li, A. Lin and F. Gan, *Surf. Coat. Technol.*, 201 (2006) 2578.
41. Fuel Cell Technologies Office, Multi-Year Research, Development and Demonstration Plan, Department of Energy, 2012.
42. L. Guo, D. Zhang, L. Duan, Z. Wang and W. H. Tuan, *Int. J. Hydrogen Energy*, 36 (2011) 6832.

© 2017 The Authors. Published by ESG (www.electrochemsci.org). This article is an open access article distributed under the terms and conditions of the Creative Commons Attribution license (<http://creativecommons.org/licenses/by/4.0/>).